

Calciothermic Synthesis of Very Fine, Hydrogenated Ti and Ti–Nb Powder for Biomedical Applications

Inge Lindemann,* Bernhard Gebel, Stefan Pilz, Margitta Uhlemann, and Annett Gebert

Due to their excellent biocompatibility, titanium and titanium–niobium alloys are especially interesting for biomedical applications. With regard to favorable near-net shape production, Ti powder synthesis is the key hurdle. Extensive research has been in progress for alternative synthesis methods since decades. Herein, an efficient alternative method to the conventional powder production process to prepare spherical powders with very small sizes ($<45\ \mu\text{m}$) for high-strength materials is shown. Very fine, hydrogenated Ti and Ti–Nb alloy powders are stable in air and are synthesized by calciothermic reduction in hydrogen. The herein presented reduction using CaH_2 starts directly from the oxides instead of chlorides. Correlations of size and morphology of the as-synthesized TiH_2 and $(\text{Ti,Nb})\text{H}_2$ powders with the precursors (TiO_2 , Nb_2O_5 , and CaH_2) are illustrated and are used to tailor the desired powders.

a small fraction after gas atomization, which is the conventional path for spherical powder fabrication.^[4] As an alternative, cheap angular Ti powder prepared by the hydride–dehydride (HDH) process can be used. It is made by crushing hydrogenated Ti sponge prepared by Kroll process. Due to its brittle nature, the intermediate TiH_2 powder shows angular morphology based on the crushing routine. Therefore, the resulting HDH Ti powder also shows angular morphology after dehydrogenation by vacuum heat treatment. But for many applications, as, e.g., MIM and the conventional press and sinter process, spherical powder is preferred to reach high packing density and low interparticle friction.^[4] In addition, for fine powders, usage of TiH_2


is advantageous as it is not as reactive toward oxygen as Ti powder. It can be easily handled in air, and contamination during the debinding step in the MIM process is hindered. Carreño-Morelli et al.^[5] tested commercial angular TiH_2 powder ($d_{50} = 20\ \mu\text{m}$) for the MIM process as fine spherical TiH_2 powder is not commercially available. The production of titanium grade 4 components was accomplished with good mechanical properties and adequate shape preservation and reproducibility. They also studied the effect of TiH_2 powder with smaller particle size ($d_{50} = 10\ \mu\text{m}$) but did not observe enhanced mechanical properties as expected. Unfortunately, sintering was performed in argon flow ($100\ \text{L h}^{-1}$). Especially the sintering of fine titanium should be conducted in vacuum,^[6] and the lower sintering temperature below $900\ ^\circ\text{C}$ should be met for limited grain growth and to prevent oxygen pickup.^[7] Consequently, using finer TiH_2 should result in nanostructured cp-Ti which is especially interesting for biomedical applications as it provides higher strength, persistent ductility, higher wear resistance, and greater cell adhesion.^[8–10] Fine and brittle TiH_2 powder might be even suitable for the conventional press and sinter process because of extensively reduced compaction force.^[11]

In addition to pure Ti, highly biocompatible Ti–Nb alloys attract increasing attention as promising implant materials in the biomedical field.^[12] Fully β -phase Ti alloys can be prepared with at least 30 at% Nb showing a comparably small Young's modulus, alleviating the stress shielding effect.^[13] Ti and Nb can form a mixed metal hydride $(\text{Ti,Nb})\text{H}_2$ with the same structure as TiH_2 with a slightly increased lattice parameter (both CaF_2 structures).^[14] Fine hydrogenated Ti–Nb powder is also used for the preparation of Ti–Nb parts by MIM or conventional press and sinter technique regarding implant applications. A new synthesis routine for fine hydrogenated Ti and Ti–Nb

1. Introduction

Titanium shows an extraordinary combination of properties such as high specific strength, excellent corrosion resistance, and biocompatibility. There are numerous applications, e.g., in the aerospace and chemical industry as well as in the biomedical field.^[1] Usage is still limited by its high-cost Kroll process originating from the high oxygen affinity and challenging workability of titanium. Therefore, near-net shape techniques are preferred for efficient material usage and reduction of conventional processing costs.^[2,3] Especially, for implant materials, higher-strength Ti materials are needed which can be achieved by grain refinement or alloying with other biocompatible elements as, e.g., Nb. Therefore, the synthesis of fine and spherical titanium or titanium alloy powder is desired with particle sizes well below $45\ \mu\text{m}$. In particular, for metal injection moulding (MIM), small and spherical particles are needed.^[1] Using MIM, complex and porous shapes can be produced easily. Unfortunately, this is only

Dr. I. Lindemann, B. Gebel, Dr. S. Pilz, Dr. M. Uhlemann, Dr. A. Gebert
Institute for Complex Materials
Leibniz IFW Dresden
Helmholtzstr. 20, Dresden 01069, Germany
E-mail: I.Lindemann@ifw-dresden.de

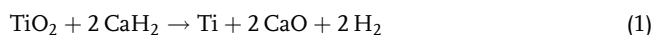
 The ORCID identification number(s) for the author(s) of this article can be found under <https://doi.org/10.1002/adem.201901210>.

© 2019 The Authors. Published by WILEY-VCH Verlag GmbH & Co. KGaA, Weinheim. This is an open access article under the terms of the Creative Commons Attribution-NonCommercial License, which permits use, distribution and reproduction in any medium, provided the original work is properly cited and is not used for commercial purposes.

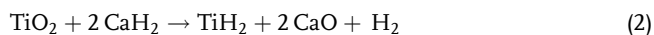
DOI: 10.1002/adem.201901210

powders is analyzed in this work. The calciothermic reduction proposed here has distinct advantages over the conventional metallurgical processes. It is possible to start from the oxide powders and obtain fine particles well below 45 μm with homogeneous elemental distribution. Therefore, high temperatures needed for melting processes are avoided which cover typical problems as segregation and dendrite structures.^[15] There are numerous alternative processes for the synthesis of Ti powders either prepared by thermochemical or by electrochemical processes starting from TiCl₄, purified TiO₂, or upgraded titanium slag (UGS).^[16] In the end, oxygen content and particle size of the powder as well as efficiency of the process are the crucial parameters.

The reduction of TiO₂ with CaH₂ known as the metal hydride reduction (MHR) process was already reported in 1966.^[17] Therein, TiO₂ is reduced according to Equation (1) at 1150–1200 °C. Due to the high reduction temperature partially sintered Ti particles in the micrometer range are obtained. In addition, 50% excess of CaH₂ is needed because of the low melting point of Ca ($T_m = 840\text{ °C}$).



Our aim is the synthesis of very fine, hydrogenated Ti particles by TiO₂ reduction with CaH₂ in H₂ atmosphere according to reaction (2) at comparably low temperatures. For that, mechanochemical reduction is used which contains the activation of the starting materials prior to heat treatment for reduction.



Recently, Zhang et al. showed the synthesis of TiH₂ powder by direct magnesiothermic reduction of TiO₂ with Mg in H₂ atmosphere at 650–800 °C.^[18] However, an additional deoxygenation treatment is needed to decrease the oxygen content of the resulting Ti powder below 2 mol%. We use Ca instead of Mg as it is a stronger reducing agent due to the higher stability of CaO. The reduction of TiO₂ with Ca is extremely exothermic and hence hard to

control. Therefore, CaH₂ is used as it shows a moderate reaction enthalpy, and it can be crushed easily in contrast to Ca.

In this work, the synthesis of very fine, highly sinter active TiH₂ powder is shown by direct calciothermic reduction of TiO₂ with CaH₂ at low temperatures. Particle size, morphology, and oxygen content of the final TiH₂ powders were evaluated in consideration of the properties shown by the starting materials. Finally, the process was also used to conduct the coreduction of TiO₂ and Nb₂O₅ to synthesize fine, hydrogenated Ti–Nb alloy powder.

2. Results

2.1. TiH₂ Powder Synthesis Starting with Anatase (Pigment TiO₂)

The starting materials were activated either in a planetary ball mill or in a shaker mill to enhance the kinetics of the solid-state reduction procedure of TiO₂ with CaH₂ according to Equation (2). The particle size of the starting oxide TiO₂ was extremely small (about 100 nm confirmed by high surface area of 9 m² g⁻¹ according to Brunauer–Emmett–Teller measurement). Typical scanning electron microscopy (SEM) images of the starting materials TiO₂ and CaH₂ before and after activation in a shaker mill (S) or rather a planetary ball mill (PBM) are shown in **Figure 1**. Evidently, the size of the TiO₂ particles did not change during the activation procedure. Instead, brittle CaH₂ was crushed easily. Its particle size was reduced extensively during activation milling. The particle size was especially small after planetary ball milling due to the higher energy impact during milling. This was also confirmed by extensive peak broadening observed in the X-ray diffraction (XRD) pattern of the planetary ball-milled powder compared with the shaker-milled powder. Those are also shown in Figure 1. After reduction (R) both activated powders contain only CaO and TiH₂. Upon removal of the byproduct CaO by leaching (RL) pure TiH₂

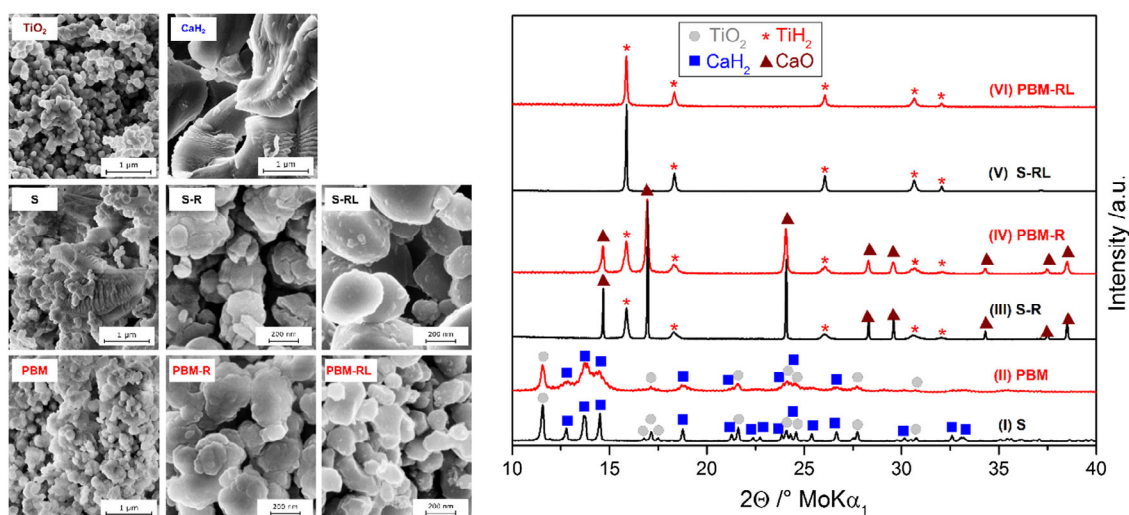


Figure 1. SEM images (left) of the starting materials CaH₂ and TiO₂ in anatase (A-TiO₂) modification. Activated mixtures after shaker milling (S) and planetary ball milling (PBM) are shown: as-milled, reduced (R), and leached (RL). Corresponding XRD patterns (right) for the as-milled activated mixtures (I–II), after reduction (III–IV), and after leaching (V–VI).

powder is obtained in both cases as proven by the XRD analysis, as shown in Figure 1. As expected, the rounded TiH_2 powder synthesized after activation in the planetary ball mill is much smaller than after activation in the shaker mill. Actually, the TiH_2 powder prepared by planetary ball-milled powder looks exactly like the TiO_2 starting material in morphology and size. This is because of the very fine CaO which acts as the particle separator and prevents sintering of the fine powder.

The oxygen content of the synthesized powder is especially sensitive to the crucible material and drying procedure. Shaker-milled TiH_2 powder reduced in a Coors high-alumina crucible (99.8% pure Al_2O_3) and dried in air at 50°C exhibited an elevated oxygen content of 4.5 mol%. Using a crucible made of conventional stainless steel (1.4301) reduced the oxygen content to 2.5 mol% for the shaker-milled TiH_2 powder dried in air at 50°C . Drying in vacuum reduced the oxygen content to only 1.3 mol% ($3.0\text{ m}^2\text{ g}^{-1}$). This value still seems comparably high but this is due the small size of the powder. The oxygen content of the commercial HDH TiH_2 powder was also comparably high with 0.7 mol% ($0.6\text{ m}^2\text{ g}^{-1}$). This powder was always handled and stored in the glovebox but the measured oxygen content did not change appreciably over time when storing it in the desiccator. Naturally, the oxygen content has a strong surface contribution as Ti forms a thin TiO_2 passivation layer. A passivation layer of 2.9 nm TiO_2 was measured for Ti powder.^[19] Therefore, this would result in an enhancement of 1.5 mol% oxygen for the shaker-milled TiH_2 with a surface area of $3.0\text{ m}^2\text{ g}^{-1}$. As suggested by Zhang et al.^[20] TiH_2 forms an even thinner oxide layer than Ti powder. Presuming a 2.0 nm TiO_2 layer seems to be reasonable with a contribution of 1.0 mol% surface oxygen for the shaker-milled TiH_2 powder ($3.0\text{ m}^2\text{ g}^{-1}$), as shown in Figure 2. This means the surface-to-volume ratio increases tremendously from 0.5% for the commercial TiH_2 powder to 2.2% for the shaker-milled TiH_2 and 6.5% for the planetary ball-milled TiH_2 , respectively.

Sintering these fine powders will produce highly activated surfaces after hydrogen desorption around 400°C . Due to the

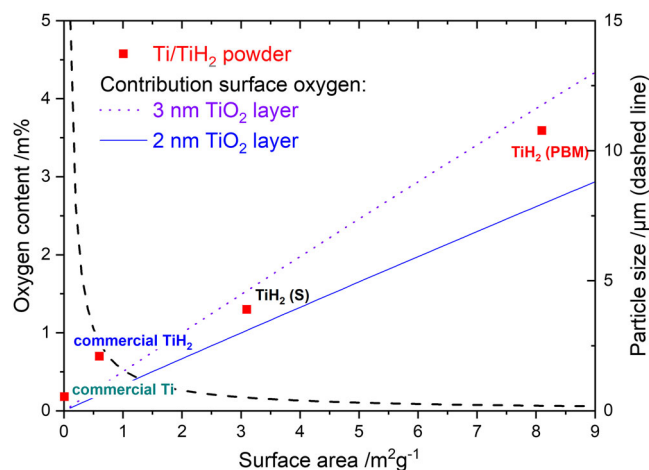


Figure 2. Oxygen content and particle size plotted versus the powder surface area for commercial and as-synthesized TiH_2 powder. In comparison, the contribution of a 2 and 3 nm TiO_2 passivation layer is shown.

surface cleaning effect, atomic hydrogen reduces the passivation layer upon diffusion from the lattice toward the surface.^[21] Cleaning of the surface by desorption of water needs to be completely before 700°C . Above this temperature, extensive oxygen diffusion into the titanium lattice starts, which makes oxygen removal impossible.^[2]

Figure 3 shows the particle size distribution of the shaker-milled and planetary ball-milled TiH_2 in comparison with cheap angular commercial TiH_2 powder and gas-atomized Ti with the smallest fraction below $45\text{ }\mu\text{m}$. Both synthesized powders show considerably smaller particles than the commercial powders. Again, it is confirmed that the planetary ball-milled TiH_2 powder is much smaller than the shaker-milled powder. The surface area was also measured to compare the synthesized powders with each other as the surface has a substantial contribution when dealing with very fine powders. The powder which was activated in the planetary ball mill has a much larger surface area of $13.6\text{ m}^2\text{ g}^{-1}$ compared with $3.0\text{ m}^2\text{ g}^{-1}$ measured for the TiH_2 powder which was activated in the shaker mill.

2.2. Effect of TiO_2 Size, Morphology, and Crystal Structure

Different TiO_2 starting materials were used to elucidate particle size and morphology dependence of the product after calciothermic reduction. Therefore, two additional types of TiO_2 starting materials were examined. Their SEM images are shown in Figure 4.

The first powder (pigment TiO_2) has anatase modification with a very high surface area of $9.0\text{ m}^2\text{ g}^{-1}$ (A- TiO_2). The other two oxide powders have a rutile structure. R- TiO_2 shows rounded morphology and a slightly smaller BET surface area ($3.6\text{ m}^2\text{ g}^{-1}$). The second type of rutile powder (RP- TiO_2) was made by heat treating the pigment anatase powder up to 1200°C in a quartz ampule. The growth of prismatic rutile needles was observed along with the crystal structure modification to rutile. This powder shows an even lower surface area of only $0.2\text{ m}^2\text{ g}^{-1}$. The hydrogen pressure was monitored while proceeding the reduction for all three different TiO_2 starting powders shaker milled with CaH_2 (see Figure 5).

In addition, desorption curves for anatase and rounded rutile after activation in the planetary ball mill are shown. For the planetary ball-milled powders, the reduction starts at already around 200°C with the subsequent desorption of TiH_2 at about 650°C and reabsorption during cooling. For shaker-milled powders of anatase and rounded rutile, the reduction reaction starts at about 500°C with subsequent H_2 desorption which is completed after 2 h at 800°C . Reduction of shaker-milled rutile needles with a smaller surface area takes much longer. Therefore, it needs extended reduction time. The reduction reaction temperature and time depend on the size of the starting materials. The particle size of the oxide starting material is important in terms of diffusion time. The reduction time increases with increasing TiO_2 particle size. The reduction temperature decreases with decreasing CaH_2 particle size. The reduction starts at lower temperature with decreasing CaH_2 particle size due to increased contact with the TiO_2 particles. This was confirmed by differential calorimetric analysis, shown in our former work, for anatase activated in the shaker mill in comparison with the planetary

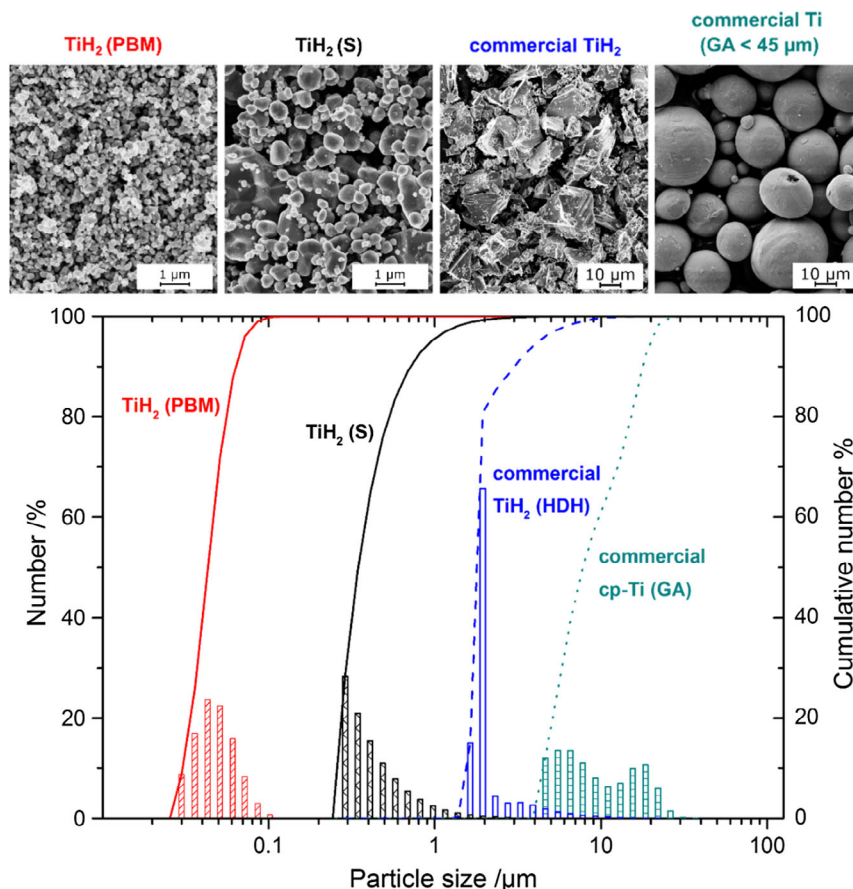


Figure 3. Particle size distribution and the corresponding SEM images of TiH_2 after calciothermic reduction activated in the planetary ball mill (PBM) or shaker mill (S) compared with commercial TiH_2 powder and the smallest fraction of gas-atomized Ti powder (<45 μm).

ball mill.^[22] The reduction product CaO preserves approximately the same size as the starting material CaH_2 . It acts as a particle separator and prevents sintering of the particles, which takes place at much lower temperatures for these fine powders. By rule of thumb, the sintering temperature is around 0.7–0.8 times the melting point of the material. But nanocrystalline Ti starts sintering already at 800 °C. The SEM images of the as-synthesized TiH_2 powders after reduction from the different TiO_2 precursors are shown in Figure 4. The morphology of the precursor oxide is transferred to the reduction product TiH_2 . The surface area of the product depends strongly on the particle size of both starting components, as shown in Table 1.

According to the SEM analysis, TiH_2 synthesized after activation in the planetary ball mill shows the same size and morphology as the corresponding precursor powder of TiO_2 . The surface area of TiH_2 is increased due to breaking of the agglomerates into aggregates during the activation procedure.^[23] The surface area of the powder activated in the shaker mill is reduced as some TiH_2 particles can aggregate due to a higher reduction temperature, longer holding time, and bigger CaO spacer particles. When starting with TiO_2 fibers, preparation of Ti fibers is possible due to transfer of morphology. These can be used for the fabrication of fiber porous metals with high porosity and small pore size for a variety of possible applications.^[24]

2.3. Synthesis of Hydrogenated Ti–Nb Powder

The coreduction of TiO_2 (9.0 $\text{m}^2 \text{g}^{-1}$) and Nb_2O_5 (3.9 $\text{m}^2 \text{g}^{-1}$) was conducted with 10 mol% excess of CaH_2 for the synthesis of hydrogenated Ti–Nb powder. A Nb content of either 17 wt% (10 at%, $x = 0.1$) or 45 wt% (30 at%, $x = 0.7$) is of special interest for biomedical applications due to the low Young's modulus expected for those compositions.^[13] Therefore, a suitable stoichiometry was chosen to perform the following reduction reaction (3)

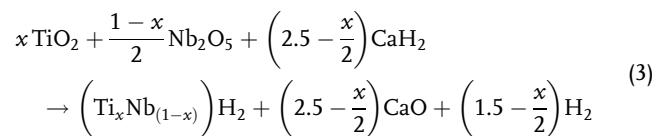


Figure 6 shows the XRD patterns of the activated powder mixture before and after reduction in Ar. The shaker-milled powders were subsequently reduced in H_2 (800 °C) for different times and washed afterward (see XRD patterns in Figure 6). The activated powder (S) exhibits only reflections of the starting materials TiO_2 , Nb_2O_5 , and CaH_2 . The reduction of the shaker-milled powder in Ar atmosphere (800 °C) results in a mixture of Ti, Nb, and CaO. The following reduction procedures were conducted in hydrogen atmosphere to synthesize the mixed (Ti,Nb) H_2 . The XRD patterns (Ti-45Nb) of the leached powders after reduction

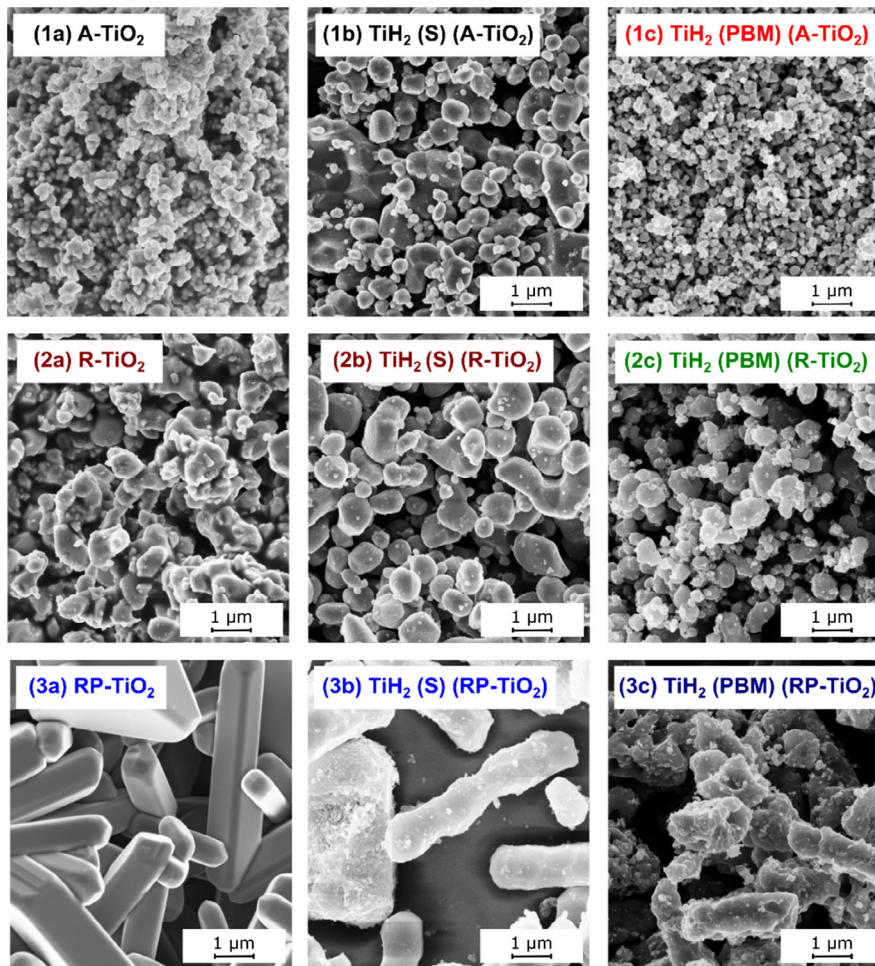


Figure 4. SEM images of different TiO_2 powders anatase (1a), rounded rutile (1b), and prismatic rutile (1c) before and after calciothermic reduction either activated in the shaker mill (S) (1-3b) or planetary ball mill (PBM) (1-3c).

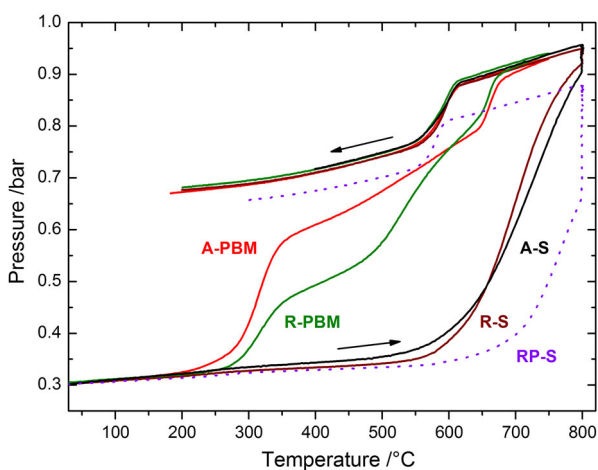


Figure 5. Desorption curves of different TiO_2 starting powders (A—anatase, R—rutile, RP—rutile prismatic) activated either in the planetary ball mill (PBM) or the shaker mill (S).

in H_2 for 2 and 5 h are also shown in Figure 6. In all cases, there is no starting material left after reduction. But, after reduction for

Table 1. Surface area ($\text{m}^2 \text{g}^{-1}$) of different TiO_2 starting materials as received and the values for the as-synthesized TiH_2 activated in the shaker mill (S) or planetary ball mill (PBM) after the calciothermic reduction of the corresponding starting oxide.

Starting material	As-received	TiH_2 (S)	TiH_2 (PBM)
A- TiO_2	9.0	3.0	13.6
R- TiO_2	3.6	2.1	8.1
RP- TiO_2	0.2	1.2	4.6

only 2 h and subsequent washing, a mixed product of Ti-rich and Nb-rich $(\text{Ti,Nb})\text{H}_2$ as well as NbH was obtained. Extending the reduction time to 5 h reduced the amount of NbH extensively. The mechanism is similar to that described in our former work for the synthesis of hydrogenated Ti–Nb alloy powder from the elements.^[14] Therein, the elements Ti and Nb were milled in hydrogen atmosphere. First, the elemental hydrides were formed (TiH_2 , NbH) and with prolonged milling duration NbH was consumed due to the incorporation of Nb into the TiH_2 lattice, forming a mixed metal hydride $(\text{Ti,Nb})\text{H}_2$. The structure of both hydrides is the same but the lattice constant of $(\text{Ti,Nb})\text{H}_2$ slightly

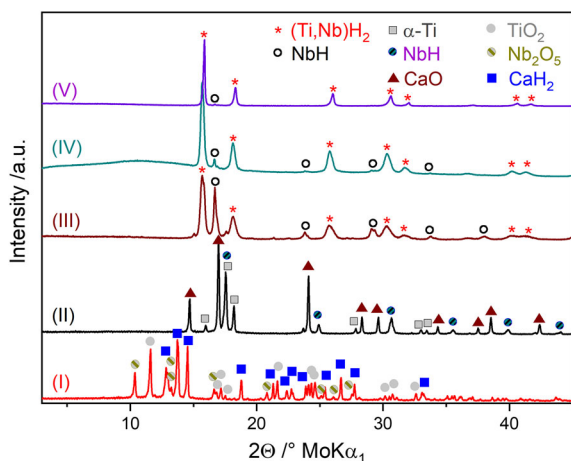


Figure 6. XRD patterns of (I) the as-milled mixture $0.1 \text{ TiO}_2 + 0.15 \text{ Nb}_2\text{O}_5 + 2.4 \text{ CaH}_2$ (II) after reduction in Ar and the leached powders (III) with $x=0.3$ after reduction in H_2 for 2 h or (IV) 4 h and (V) $x=0.1$ after reduction for 2 h.

increases with increasing Nb incorporation. Therefore, longer diffusion time is needed to end up with a completely homogeneous hydrogenated Ti–Nb powder. Even after reduction for 5 h, there is still a reflection of NbH visible. The driving force for the diffusion is reduced with a lower concentration gradient. In contrast, the powder with lower Nb content (Ti-17Nb) is synthesized already after 2 h (see pattern (V) in Figure 6). Thus, with higher Nb content, a longer reduction time is needed which leads to a slightly reduced surface area of the product. After a reduction time of 2 h, a surface area of $3.8 \text{ m}^2 \text{ g}^{-1}$ was measured compared with only $2.2 \text{ m}^2 \text{ g}^{-1}$ after reduction for 5 h. The particle size distribution was measured for the sample reduced for 5 h in comparison with the TiH_2 (S) powder reduced for 2 h (see Figure 7). The size of the powders is comparable. The inset of Figure 7 shows the SEM images of $(\text{Ti,Nb})\text{H}_2$ compared with TiH_2 (S). Size and morphology of both powders are similar. The flow of the particles is quite reasonable as the small particles form

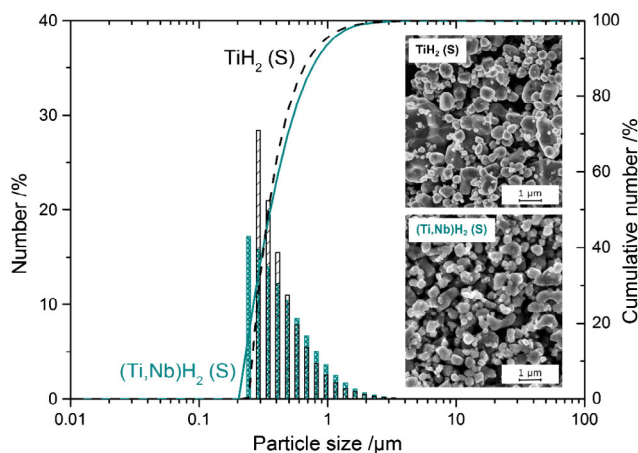


Figure 7. Particle size distribution of TiH_2 (S) compared with $(\text{Ti,Nb})\text{H}_2$ (S). Inset: SEM images of the corresponding loose powders.

macroflakes due to the wet chemical filtration procedure with the formation of $\text{Ca}(\text{OH})_2$ and calcium acetate as flocculation agents. Therefore, the powders are even suitable for conventional press and sinter approach.

3. Conclusion

Calciothermic synthesis of very fine hydrogenated Ti and Ti–Nb powder was successful under moderate conditions in hydrogen atmosphere. The size and morphology of the final powder products can be tailored by the size and morphology of the starting materials and the used activation routine. This is the only process known to the authors to produce rounded TiH_2 and $(\text{Ti,Nb})_2$ powders with such small sizes well below $45 \mu\text{m}$. The measured oxygen content of the reduction products was comparably high due to extraordinary high surface area of the fine agglomerated powder particles ($2.2\text{--}13.6 \text{ m}^2 \text{ g}^{-1}$). Nevertheless, the surface cleaning effect during the sintering process in vacuum will remove the passivation layer by choosing an appropriate heating ramp.^[25] Therefore, fine-grained Ti and Ti–Nb specimens can be prepared by either the conventional press and sinter technique or MIM. Thus, these fine brittle hydrogenated powders are especially interesting in the biomedical field.

4. Experimental Section

Synthesis: Pigment TiO_2 powder in anatase modification (Sigma Aldrich, 99.9%, -325 mesh), TiO_2 in rutile modification (Alfa Aesar, min. 99.5%, $1\text{--}2 \mu\text{m}$ APS), and Nb_2O_5 (Sigma Aldrich, 99.9%, -325 mesh) were used for reduction experiments. CaH_2 (Alfa Aesar, 90–95%, 2 mm and down) was used as the reductant. The entire synthesis procedure contained three main steps: 1) Activation: The activation of the starting powders of TiO_2 with CaH_2 in the ratio 1:2.2 (10 mol% excess of CaH_2) was conducted in Ar atmosphere either in a shaker mill (S) or in a planetary ball mill (PBM). The following parameters were used: shaker mill (Retsch MM200): 25 Hz, 3 min, $V = 10 \text{ mL}$, 1 g, 1 SS ball ($\varnothing 10 \text{ mm}$) and planetary ball mill (Fritsch P6): 200 rpm, 15 h, $V = 220 \text{ mL}$, 6 g, 55 SS balls ($\varnothing 10 \text{ mm}$). 2) Reduction (R): The reduction synthesis was conducted with a starting pressure of 0.3 bar H_2 atmosphere with the filled crucible inside a quartz glass tube monitoring reduction reaction pressure with a Si chip. The shaker-milled powder (S) was reduced at 800°C for 2 h, and the planetary ball-milled powder (PBM) was only heated to 750°C for 1 h. 3) Leaching: Handling and storing of the materials were done in an Ar glovebox up to the leaching procedure. Then, for removal of the CaO byproduct, the powders were handled in air. Therefore, the reduction product was dissolved and stirred in deionized water (DI). Afterward, it was leached with diluted acetic acid (5%) and washed with a large volume of DI water using a membrane filter from Pall Corporation (Versapor $<0.8 \mu\text{m}$). Washing was completed with ethanol followed by drying in vacuum.

Characterization: The particle size distribution was measured with a Microtrac Bluewave particle sizer in aqueous solution and addition of 1 mol% SDS for the very fine powder synthesized by calciothermic reduction. The surface areas of the powders were analyzed by the BET method with a Quadrasorb SI (Quantachrome) by 5-point BET ($p/p_0 = 0.1, 0.15, 0.2, 0.25, \text{ and } 0.3$). The imaging of the powders on carbon tape was done with SEM (LEO Gemini, 10 kV, InLens). Structural analysis was conducted by XRD with a STOE Stadi with $\text{MoK}\alpha_1$ ($\lambda = 0.70926 \text{ nm}$) radiation.

Acknowledgements

This work was supported by the German Research Foundation (DFG) (LI 2536/1-1). The authors thank Andrea Voß for chemical analysis and Heike Bußkamp for oxygen analysis.

Conflict of Interest

The authors declare no conflict of interest.

Keywords

ball milling, biomedicines, hydrides, material synthesis, titanium powders

Received: October 8, 2019

Revised: October 30, 2019

Published online: December 9, 2019

-
- [1] *Titanium Powder Metallurgy - Science, Technology and Applications*, (Eds: M. Qian, F. H. Froes), Butterworth-Heinemann, Oxford/Stoneham, MA **2015**, pp. 601–608.
- [2] M. Qian, *Int. J. Powder Metall.* **2010**, 46, 29.
- [3] F. H. Froes, D. Eylon, *Int. Mater. Rev.* **1990**, 35, 162.
- [4] P. Sun, Z. Z. Fang, Y. Zhang, Y. Xia, *JOM* **2017**, 69, 1853.
- [5] E. Carreño-Morelli, J.-E. Bidaux, M. Rodríguez-Arbaizar, H. Girard, H. Hamdan, *Powder Metall.* **2014**, 57, 89.
- [6] R. S. Dean, J. R. Long, F. S. Wartman, E. L. Anderson, *Trans. AIME* **1946**, 166, 369.
- [7] H. T. Wang, M. Lefler, Z. Z. Fang, T. Lei, S. M. Fang, J. M. Zhang, Q. Zhao, *Key Eng. Mater.* **2010**, 436, 157.
- [8] S. G. Steinemann, *Injury* **1996**, 27, S-C16.
- [9] R. Z. Valiev, I. P. Semenova, V. V. Latysh, H. Rack, T. C. Lowe, J. Petruzzelka, L. Dluhos, D. Hrusak, J. Sochova, *Adv. Eng. Mater.* **2008**, 10, 8.
- [10] I. Lindemann, P. Langhelm, R. Schmidt, A. Gebert, in *Proc. of Euro PM 2018: (International Powder Metallurgy Congress & Exhibition)*, Bilbao, **2018**.
- [11] I. M. Robertson, G. B. Schaffer, *Powder Metall.* **2010**, 53, 12.
- [12] D. Zhao, K. Chang, T. Ebel, M. Qian, R. Willumeit, M. Yan, F. Pyczak, *J. Mech. Behav. Biomed. Mater.* **2013**, 28, 171.
- [13] T. Ozaki, H. Matsumoto, S. Watanabe, S. Hanada, *Mater. Trans.* **2004**, 45, 2776.
- [14] I. Lindemann, R. Schmidt, S. Pilz, B. Gebel, A. Teresiak, A. Gebert, *J. Alloys Compd.* **2017**, 729, 1244.
- [15] M. A. Gepreel, M. Niinomi, *J. Mech. Behav. Biomed. Mater.* **2013**, 20, 407.
- [16] Z. Z. Fang, J. D. Paramore, P. Sun, K. S. R. Chandran, Y. Zhang, Y. Xia, F. Cao, M. Koopman, M. Free, *Int. Mater. Rev.* **2018**, 63, 407.
- [17] B. A. Borok, V. G. Teplenko, in *Researches in Powder Metallurgy*, Consultants Bureau, New York **1966**, pp. 3–14.
- [18] Y. Zhang, Z. Z. Fang, P. Sun, T. Zhang, Y. Xia, C. Zhou, Z. Huang, *JACS* **2016**, 138, 6916.
- [19] Y. Xia, Z. Z. Fang, P. Sun, Y. Zhang, T. Zhang, M. Free, *J. Mater. Sci.* **2017**, 52, 4120.
- [20] Y. Zhang, Z. Z. Fang, Y. Xia, P. Sun, B. V. Devener, M. Free, O. High, *Chem. Eng. J.* **2017**, 308, 299.
- [21] O. M. Ivasishin, D. Eylon, V. I. Bondarchuk, D. G. Savvakina, *Defect Diffus. Forum* **2008**, 277, 177.
- [22] I. Lindemann, M. Herrich, B. Gebel, R. Schmidt, U. Stoeck, M. Uhlemann, A. Gebert, *Scr. Mater.* **2017**, 130, 256.
- [23] U. Gesenhues, *J. Nanopart. Res.* **1999**, 1, 223.
- [24] Z. Xi, J. Zhu, H. Tang, Q. Ao, H. Zhi, J. Wang, C. Li, *Materials* **2010**, 4, 816.
- [25] O. M. Ivasishin, D. G. Savvakina, M. M. Gumenyak, O. B. Bondarchuk, *Key Eng. Mater.* **2012**, 520, 121.